Energy and Buildings 81 (2014) 381–390

Contents lists available at ScienceDirect

Energy and Buildings

journal homepage: www.elsevier.com/locate/enbuild

Modeling of a direct expansion geothermal heat pump using artificial neural networks

Jean-Louis Comlan Fannou*, Clément Rousseau, Louis Lamarche, Stanislaw Kajl

Thermal Technology Center (TTC), Department of Mechanical Engineering, École de technologie supérieure, Université du Québec, 1100, Notre-Dame Street West, Montreal H3C 1K3, Canada

ARTICLE INFO

Article history:
Received 23 May 2014
Accepted 25 June 2014
Available online 2 July 2014

Keywords:
Modeling
Geothermal
Heat pump
Direct expansion
Neural network
Heating

ABSTRACT

The real potential for energy savings exists in heating, ventilation, and air conditioning systems in general, and especially in geothermal heat pumps systems. Recent studies indicate that a mere 1% improvement in the efficiency of such systems generates millions of dollars in savings at the national level. This efficiency can be optimized when better control strategies are implemented. A first step in the control and optimization process is to establish a model that describes the system's behavior. In this study, artificial neural networks were selected for modeling a particular type of heat pump called direct expansion geothermal heat pump because the ground heat exchanger is a component of the heat pump, and thus directly plays the role of condenser or evaporator according to the operation mode. The data collection methodology and the algorithms used for training are presented. Of the four algorithms tested in this study with variable numbers of neurons in the hidden layers, the model obtained using the Levenberg–Marquardt (LM) algorithm with 28 neurons in the hidden layer appears to be the best, with an average coefficient of multiple determinations of about 0.9991, an average RMS of 0.16330, and an average COV of 2.9319.

1. Introduction

In recent years, artificial neural networks (ANN) have become an alternative to traditional methods of statistical data analysis in several disciplines of human activity, including in economics, ecology and environment [1], biology and medicine. They are used to solve the problems of classification, prediction, modeling, control, optimization, categorization, pattern recognition and associative memory [2]. In the specific context of data processing, the ANN is an approximation method of complex systems that are difficult to model using traditional methods [3]. The modeling process of dynamic systems using conventional approaches (analytical and experimental validation) begins by first establishing all the governing equations of all physical phenomena characterizing the system as a function of parameters and multiple variables; the numerical methods needed to solve these equations are then chosen based on assumptions, and sometimes, in the case of heat transfer, by adjusting correlations transfer coefficients available in the literature to obtain a better model in agreement with the experimental data. This exercise can sometimes be difficult and complex to realize [4]. ANN therefore offers alternatives to these conventional methods of overcoming their limitations using approaches based on experimental data, and allows the extraction of nonlinear implicit relationships between the desired input–output variables that cannot be obtained by conventional methods [5]. The principle is very simple, and consists of a learning phase during which the various components of the network are evolving until the network has completed the desired task followed by the use phase, where the model is tested with a new input value. However, for the ANN to provide a reliable prediction model, data to be processed must be representative of the system [6], hence the need to clearly define the problem and to elaborate the experimental process for collecting data.

ANN works by distributing the values of variables in automata called neurons by analogy with human neurons. These units are organized in architecture: input layer–hidden layer–output layer connected to each other by connections with associated weights. The network output is calculated using a transfer function whose choice depends on the type of input variables used. When the inputs are positive, the function of the log-sigmoid transfer is used, and when data has negative values, the sigmoid tangent function is operated [4,7].

* Corresponding author at: École de technologie supérieure, Mechanical Engineering Deptment, 1125 William St., Montreal H3C 1P7, Canada.
Tel.: +1 514 396 8858.
E-mail addresses: jean-louis.fannou.1@ens.etsmtl.ca (J.-L.C. Fannou), clement.rousseau.2@ens.etsmtl.ca (C. Rousseau), louis.lamarche@etsmtl.ca (L. Lamarche), stanislaw.kajl@etsmtl.ca (S. Kajl).

http://dx.doi.org/10.1016/j.enbuild.2014.06.040
0378-7788/

Nomenclature

COP	coefficient of performance for heating
T_{wi}	cooling water inlet temperature (°C)
T_{wo}	cooling water outlet temperature (°C)
P_{fi}	inlet pressure of the geothermal evaporator (kPa)
T_{fi}	inlet temperature of the geothermal evaporator (°C)
P_{fo}	outlet pressure of the geothermal evaporator (kPa)
T_{fo}	outlet temperature of the geothermal evaporator (°C)
P_{dis}	discharge pressure (kPa)
C_{pw}	heat capacity of water (J/kg K)
$\dot{m}$	cooling water flow rate (kg/s)
W_c	power consumed by the compressor (W)
Q_h	heating capacity (W)
N	number of neurons in the hidden layer
N_s	number of loop selected
T_i	start time (min)
T_f	stop time (min)
T_s	simulation time (s)
BNHL	best neurons number in hidden layer

The overall objective of the ANN is to find the best weight configuration of connections between neurons used to associate an appropriate output for each input configuration.

In the specific areas of refrigeration, air conditioning and heat pumps (RACHP), ANN is often used as follows:

- Modeling and prediction of vapor compression systems,
- Modeling of refrigeration system and heat pump components,
- Modeling and prediction of vapor absorption systems,
- Prediction of the properties of refrigerants,
- Control RACHP,
- Heating and air conditioning systems,
- Energy analysis of a building.

Most of the applications of ANN in RACHP and energy analysis are summarized by Mohanraj et al. [4] and Kumar et al. [6]. The different network architectures used are: multi-layer feed forward, radial biased function network, generalized regression neural network and adaptive neuro fuzzy systems. However, the most commonly used is the multi-layer feed forward network, with its popular learning back-propagation algorithm (BPA).

In this study, we use an ANN model to predict the performance (heating capacity and the coefficient of performance) of a particular type of geothermal heat pump (GHP) called a direct expansion (DX) heat pump (Fig. 1). The geothermal heat pump has attracted renewed interest over the last decade because of the advantages it offers as compared to its secondary loop (SL) counterpart [8] (Fig. 2). While geothermal secondary loop systems design methods and simulation tools are available in the literature [9–12], those of DX heat pumps are still only covered in experimental studies. The performance prediction of a thermal system is a prerequisite for its design, process optimization and control, which is why the ANN is recommended for estimating the performance of thermal systems in engineering applications [5]. In addition, there is a real energy savings potential in geothermal systems when a good control policy is provided for efficient use [13]. For example, a mere 1% improvement in the energy efficiency of these systems resulted in annual savings of millions of dollars nationwide [14], and our recent study shows that the direct expansion geothermal heat pump can provide 70% energy savings as compared to electricity [15]. However, the first step in a process control is the identification and modeling of the system to predict its behavior. The work presented here is part of this, and therefore proposes an ANN model that can be used even online to simulate and develop appropriate control strategies for DX heat pump. Although there are few publications on the DX heat pump in the literature as compared to its secondary loop counterpart (Fig. 1) over the past decade, some works on DX heat pumps systems have indeed been done. The list of research works summarized by [15], as well as those on secondary loop systems, are listed by Esen and Inalli [16].

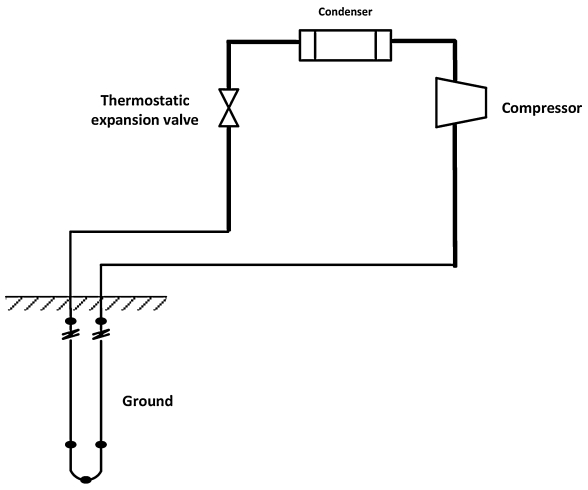

Fig. 1. Schematic of a direct expansion geothermal heat pump (DX).

2. Methodology

2.1. Using of the model

The aim of this work is to model a DX heat pump capable of adapting DX heat pump operation to real building loads. Indeed, there is a potential for energy savings in GSHP when a good control is assured. [13]. This ANN model will thus be integrated into the development of an Intelligent Building System (IBS) which uses a supervisor and a coordinator to set control strategies for local controllers [17]. More specifically, it can be integrated into simulation tools of DX heat pump systems as a model of behavior or to create a neural network loop to perform an adaptive control [18], and finally, as a reference model to adapt other DX heat pumps used in real time [14,17]. In the latter case, it will be necessary to implement a real-time training algorithm based on the recursive least

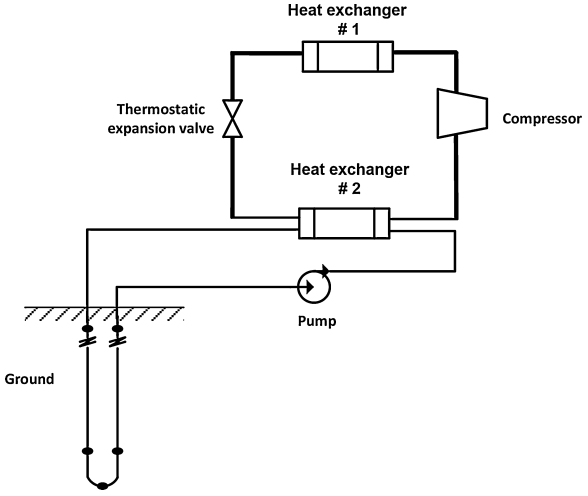

Fig. 2. Schematic of a traditional secondary loop geothermal heat pump.

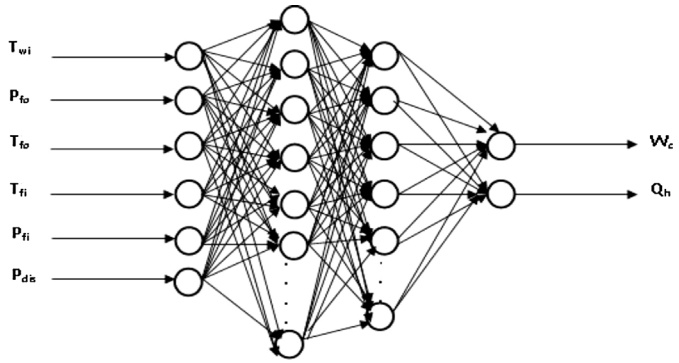

Fig. 3. Diagram of ANN model.

squares (RSL) method, and whose role is to adjust the weights of the reference model network. The details of this strategy of training algorithm can be found, for example, in the works of Teeter and Mo-Yuen [14], Guang-Bin et al. [19] and Pierre et al. [18].

2.2. Model inputs–outputs selection

Insofar as the ANN model (Fig. 3) will serve as a simulation tool for evaluating performance and as a behavior model for developing efficient control strategies for the DX heat pump system, the input variables chosen are those that can be measured online on the DX heat pump, and which have an influence on system performance. Thus the model input corresponds to the parameters that define the thermodynamic state of the DX heat pump.

The following inputs are selected:

- The temperature and pressure at the inlet of the DX geothermal evaporator (T_{fi}, P_{fi})
- The temperature and pressure at the outlet of the DX geothermal evaporator (T_{fo}, P_{fo})
- The inlet temperature of cooling water in the condenser (T_{wi})
- The discharge pressure (P_{dis})

The outputs studied are the Q_h (heating capacity) and W_c (compressor power consumption) of the DX heat pump. These two outputs characterize the performance of the heat pump to the extent that their report defines the coefficient of performance (COP).

2.3. Data collection methodology

The objective is to establish the most representative model of the DX heat pump in order to facilitate broader use. It is therefore important to vary the input parameters of the model within acceptable limits to provide reliable and representative data from the operation of the DX heat pump. Thus, four variables were modified throughout the tests:

- The length of geothermal loops (number of selected loops), by varying the length of the geothermal wells, the conditions of heat transfer between the grout and pipe (a reduction in length may decrease the heat extracted, for example) changed, and the input and output were therefore varied [20].
- The conditions of ground temperature by activation the loops which had same length but different loop schedule operation. Our experimental device, which consisted of three parallel geothermal loops installed in wells, could be activated separately. When two loops are selected (loops No. 1 and 2, for example), loop No. 3 is at rest, and so the soil temperature in the loop remains high, as compared to those of loops No. 1 and 2. When loops No. 2 and 3 are active following loops No. 1 and 2, many start conditions change relative to the latter operation period, which leads to a variation of inputs, and therefore, of the output variables.
- The flow rate of cooling water in the condenser. An increase in this flow rate causes an increase in the heating capacity and a decrease in the condensation pressure, leading to an increase in COP [15]. The signal for controlling the opening of the mixing valve (Belimo valve) is installed on the distribution circuit, which allows a variation of the inlet temperature of the cooling water; when this temperature rises, it leads to an increase in the condensation pressure, and consequently, to decreased performance.

In all cases, a variation of one of these parameters results in a change in the thermodynamic state of the DX heat pump. The inputs and outputs are thus modified.

3. Experimental set-up and results

The direct expansion geothermal heat pump used in this study is a model DXWG-45 unit by the Maritime Geothermal Company (Fig. 4). The details concerning the components and operations of the device are contained in the experimental section of Fannou et al. [15]. In this study, the DX heat pump is used only in heating mode (Fig. 5).

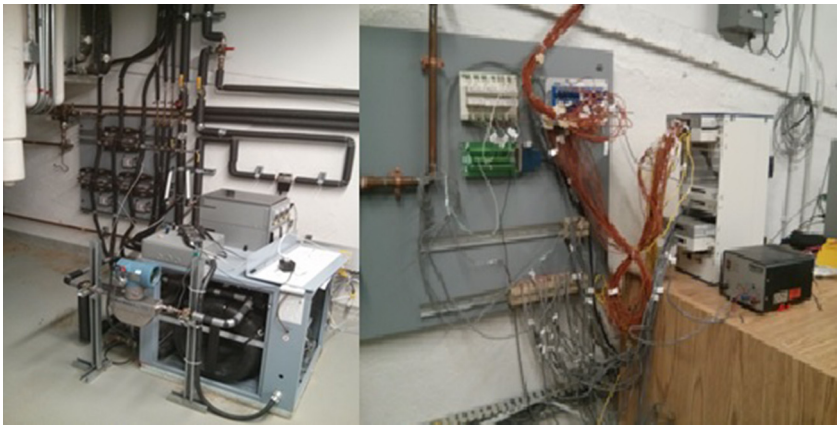

Fig. 4. Photos of direct expansion geothermal heat pump and data acquisition panel.

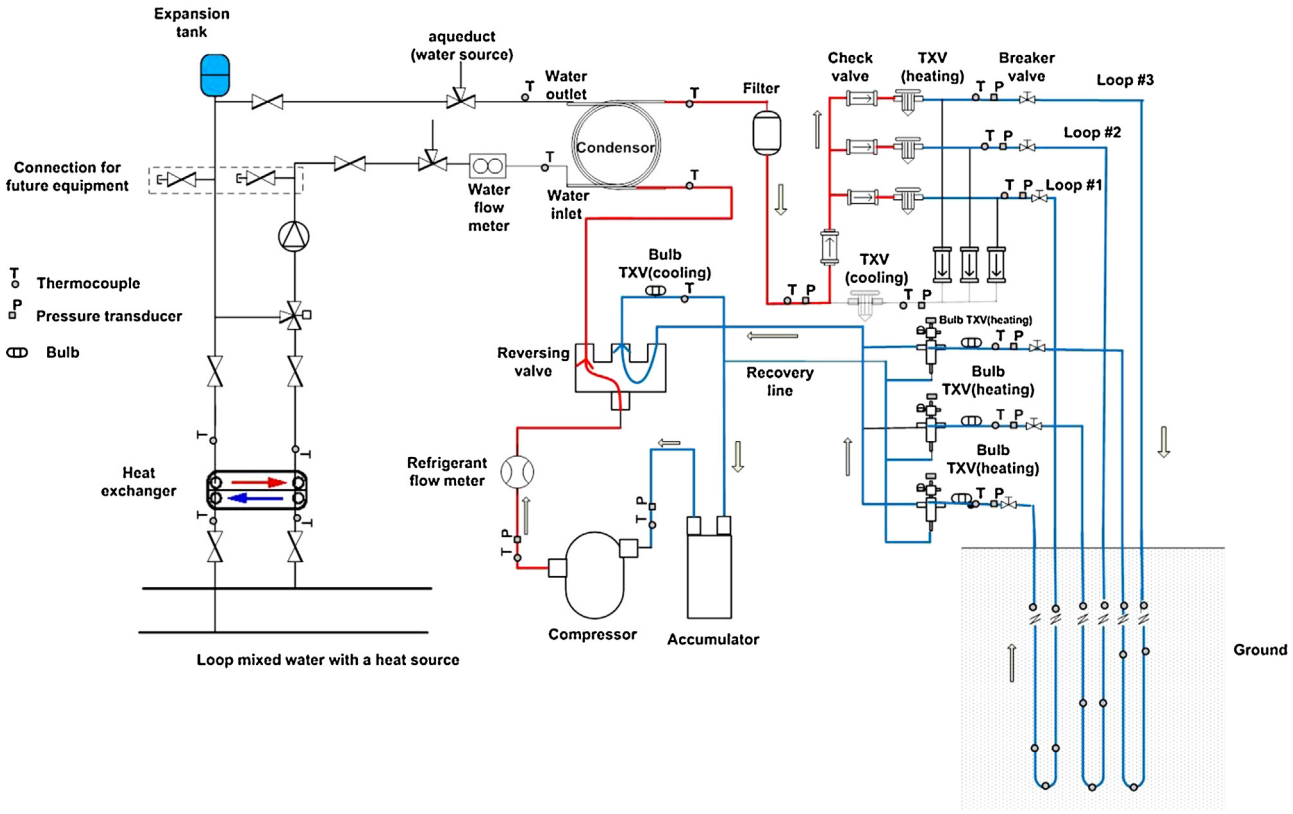

Fig. 5. Schematic diagram of the experimental device in heating mode.

Table 1
Variables and set points.

Variable	Set point		
Flow rate (kg s^{-1})	0.19	0.32	0.44
Valve opening (%)	0	40	70
Number of DX GHE selected	1	2	3

3.1. Data collection procedure

According to Table 1, nine tests are carried out to establish the database according to the optimal design plan proposed by Taguchi [21]. This experimental strategy distinguishes this study from the previous ones which only vary one parameter of the system to establish their database [5]. The database obtained thus includes all possible DX heat pump behaviors, and thus facilitates the portability of the resulting model. Table 2 shows the different tests performed during the winter of 2010 and 2014. Each test took about 20–30 h. In addition, two special types of tests were conducted and added to the database: (i) a continuous operation of the heat pump with two active loops by changing the opening of the Belimo valve (Test No. 10), (ii) a sequence of continuous operation of the pump with the change of the number of loops as shown in Fig. 6 (Test No. 11). Table 3 shows the time sequences.

Table 2
Test planning in heating mode.

Test No.	Opening of the valve (%)	$\dot{m}_w$	N_s	DX GHE selected
1	0	0.19	1	Loop # 1
2	0	0.32	2	Loop # 1 & Loop # 2
3	0	0.44	3	Loop # 1 & Loop # 2 & Loop # 3
4	40	0.19	2	Loop # 2 & Loop # 3
5	40	0.32	3	Loop # 1 & Loop # 2 & Loop # 3
6	40	0.44	1	Loop # 2
7	70	0.19	3	Loop # 1 & Loop # 2 & Loop # 3
8	70	0.32	1	Loop # 3
9	70	0.44	2	Loop # 1 & Loop # 3
10	Variable	0.44	2	Loop # 1 & Loop # 3
11	0	0.44	Variable	Variable

Table 3
Operation time sequence.

Sequence	T_i	T_f
Loops #1 & 2	0	132
Loops #1 & 3	132	258
Loops #2 & 3	258	379
Loops #1, 2 &3	379	1246
Loop #1	1246	1358
Loop #2	1358	1439
Loop #3	1439	1577

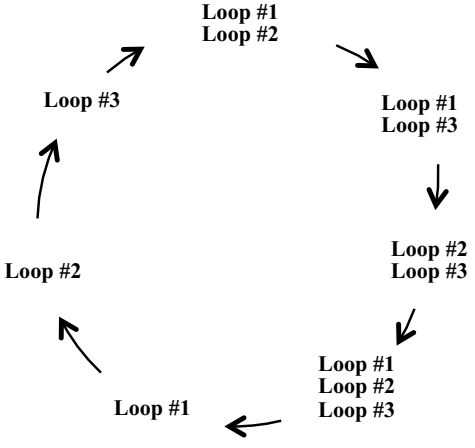

Fig. 6. Loop sequence diagram.

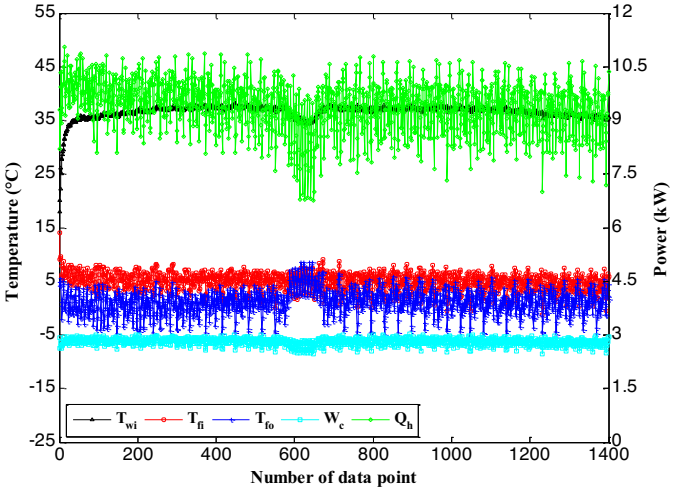

Fig. 7. Variations of input (temperature) and output for Test No. 3.

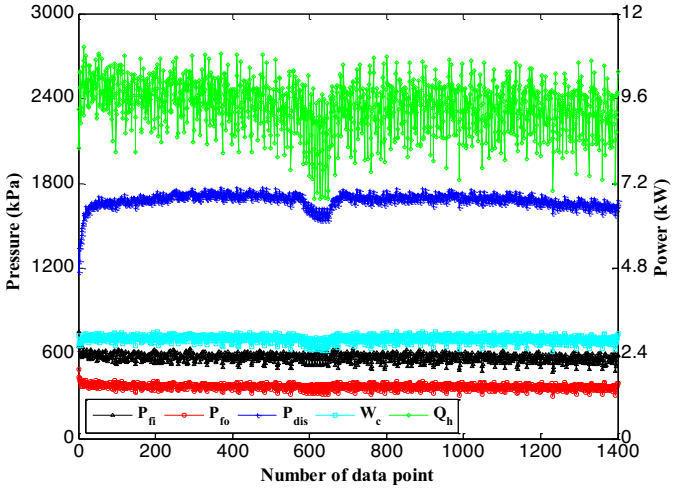

Fig. 8. Variations of input (pressure) and output for Test No. 3.

It should be noted that the correctly calibrated temperature sensors and pressure installed in the circuit provide the measurements at different points of the circuit (see Fig. 5). Data acquisition and recording are managed in the Labview software environment.

3.2. Data reduction and experimental results

3.2.1. Data reduction

The coefficient of performance and heating capacity are calculated as follows:

$$Q_h = \dot{m}_w Cp_w (T_{wo} - T_{wi}) \quad (1)$$

The power consumed by the compressor W_c is measured.

The coefficient of performance of the heat pump can be calculated by:

$$COP = \frac{Q_h}{W_c} \quad (2)$$

3.2.2. Experimental results

The database obtained by performing tests numbered from 1 to 11 was very large (19,995 × 6 points for input and 19,995 × 2 points for output). That is why we chose to present only the results of Tests Nos. 3, 6, 10 and 11 as an indication, and later specify the range of inputs and outputs that defined the experimental domain of this study. Moreover, for each test, the average number of points was about 1817. Further, to make the figures readable, we chose to present some of the experimental data.

Figs. 7 and 8 show part of the experimental data of the Test No. 3 (Table 2), in which the Belimo valve opening is set at 0%, the cooling water flow rate is 0.44 kg s^{-1} and the three geothermal loops are in operation. Fig. 7 shows the variations of inputs (temperature) and outputs and Fig. 8 presents changes in inputs (pressure) and the outputs for the various operating points of the DX heat pump. For the test set, the temperature of the cooling water in the condenser inlet is between 16.6 °C and 38.2 °C, and the pressure and temperature of the refrigerant at the inlet of the geothermal evaporator are between 459 kPa and 752 kPa, −1.5 °C and 14.1 °C, respectively. The pressure and temperature of the refrigerant at the outlet of the geothermal evaporator are between 286 kPa and 487 kPa, −6.4 °C and 8.6 °C respectively. The discharge pressure of the compressor is between 1141 kPa and 1771 kPa. The W_c and Q_h are between 2.35 kW and 3.02 kW, 6.3 kW and 12 kW, respectively.

Figs. 9 and 10 show part of the experimental data of Test No. 6 (Table 2), in which the Belimo valve opening is set at 40%, the cooling water flow rate is 0.44 kg s^{-1} and one loop is selected (loop No. 1). Fig. 9 shows the variations of inputs (temperature) and outputs and Fig. 10 presents changes in inputs (pressure) and outputs for the different operating points of the DX heat pump. For the test set, the temperature of the cooling water to the condenser inlet is set between 24 °C and 31.3 °C, and the pressure and temperature

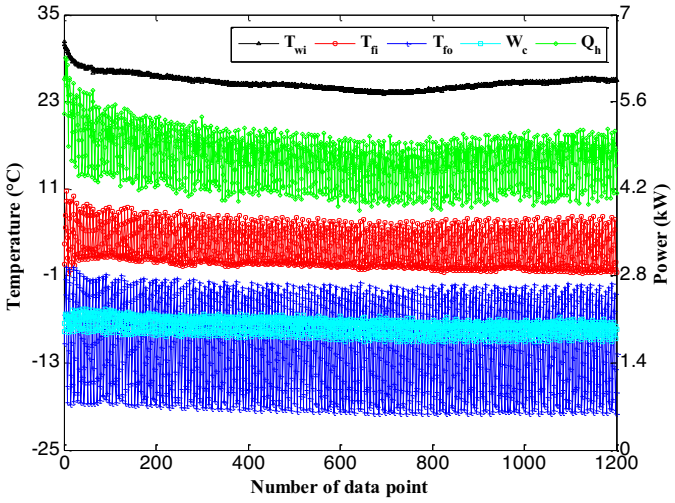

Fig. 9. Variations of input (temperature) and output for Test No. 6.

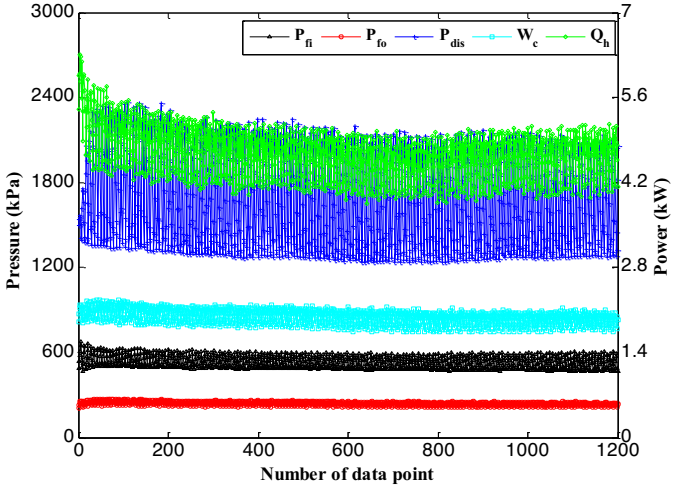

Fig. 10. Variations of input (pressure) and output for Test No. 6.

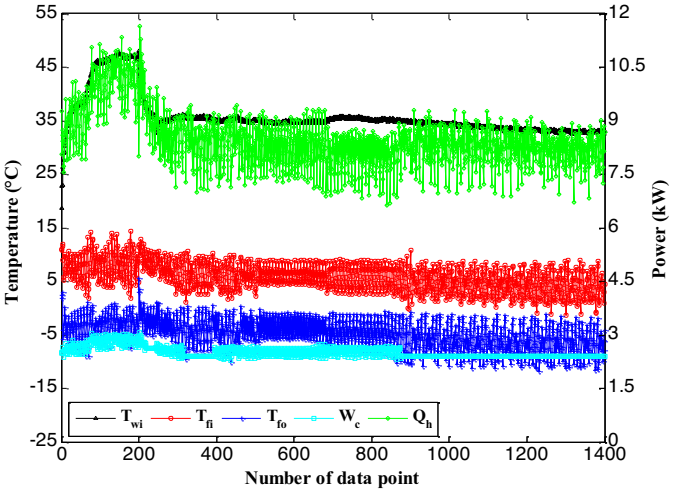

Fig. 11. Variations of input (temperature) and output for Test No. 10.

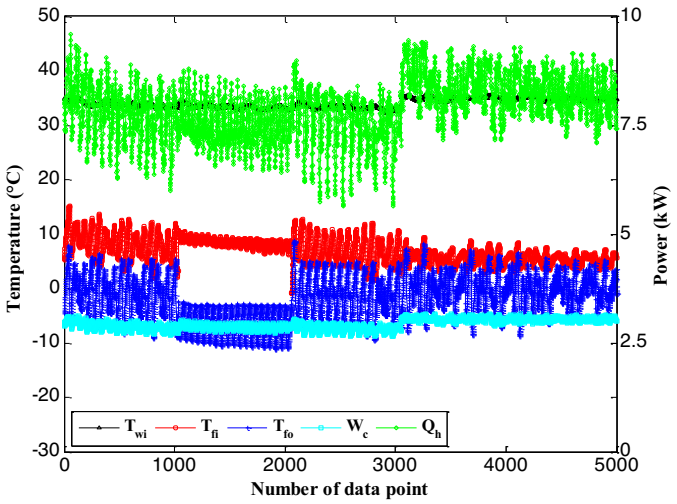

Fig. 13. Variations of input (temperature) and output for Test No. 11.

of the refrigerant at the inlet of the geothermal evaporator is between 466 kPa and 674 kPa, and −1 °C and 10.6 °C respectively. The pressure and temperature of the refrigerant at the outlet of the geothermal evaporator are between 208 kPa and 271 kPa, and −20.1 °C and 1 °C, respectively. The discharge pressure of the compressor is between 1227 kPa and 2364 kPa, and the W_c and Q_h are between 1.72 kW and 2.26 kW, 3.7 kW and 6.3 kW, respectively.

Figs. 11 and 12 show part of the experimental data of Test No. 10, for which the valve opening varies by 13%, 25%, 50% and 70%, continuously. This is Test No. 9 (Table 2), where the opening of the valve has been varied in order to obtain a greater cooling water inlet temperature range. Fig. 11 shows the variations of inputs (temperature) and outputs and Fig. 12 presents changes in inputs (pressure) and outputs for the various operating points of the DX heat pump. For the test set, the temperature of the cooling water at the condenser inlet is between 18.7 °C and 48 °C, and the pressure and temperature of the refrigerant at the inlet of the geothermal evaporator are between 462 kPa and 760 kPa, −1.3 °C and 14.4 °C, respectively. The pressure and temperature of the refrigerant at the outlet of the geothermal evaporator are between 270 kPa and 396 kPa, −11.7 °C and 5.6 °C, respectively. The discharge pressure of the compressor is between 1145 kPa and 2236 kPa. The W_c and Q_h are between 2.23 kW and 3.06 kW, 6.6 kW and 11.6 kW, respectively.

Figs. 13 and 14 show part of the experimental data of Test No. 11 for which the Belimo valve opening is set at 0%, the cooling water flow rate is 0.44 kg s^{-1} and with an activation sequence of geothermal loops shown in Fig. 6. The duration of each sequence is shown in Table 3. This test is particularly important as it provides the performance of the DX heat pump in continuous operation, depending on the number of loops activated. These data are very useful in the control process and optimization because they allow the adaptation of the DX heat pump operations, depending on the heat demand.

Fig. 13 shows the variations of inputs (temperature) and outputs and Fig. 14 presents changes in inputs (pressure) as a function of the outputs for the various operating points of the DX heat pump. For the test set, the temperature of the cooling water to the condenser inlet is between 29.1 °C and 35.8 °C, and the pressure and temperature of the refrigerant at the inlet of the geothermal evaporator are between 457 kPa and 775 kPa, −1 °C and 15 °C, respectively. The pressure and temperature of the refrigerant at the outlet of the geothermal evaporator are between 218 kPa and 407 kPa, −19.4 °C and 8.7 °C, respectively. The discharge pressure of the compressor is between 1330 kPa and 2459 kPa. The W_c and Q_h are between 2.32 kW and 3.17 kW, 3.7 kW and 9.6 kW, respectively. Finally, Fig. 15 shows the overall results of the DX heat pump in heating mode and Fig. 16 shows the mean average values of the coefficient of performance, power consumed by the compressor and heating capacity versus the loop sequence for this test.

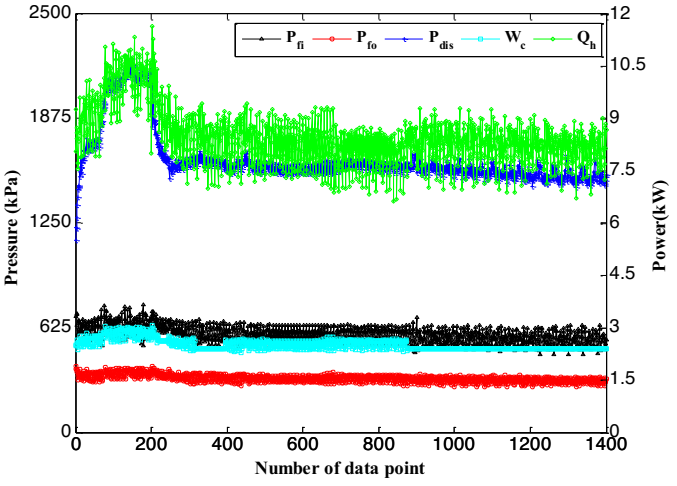

Fig. 12. Variations of input (pressure) and output for Test No. 10.

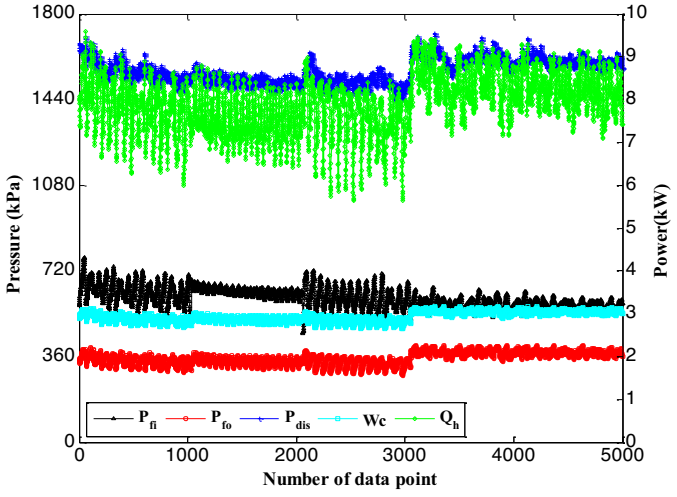

Fig. 14. Variations of input (pressure) and output for Test No. 11.

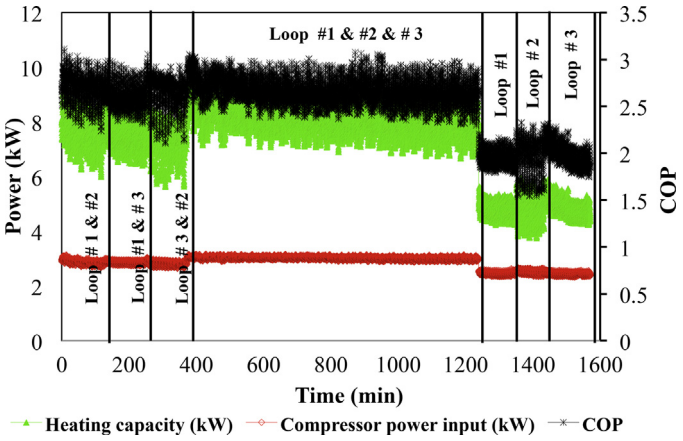

Fig. 15. Global variations of Q_h, W_c and the COP (Test No. 11).

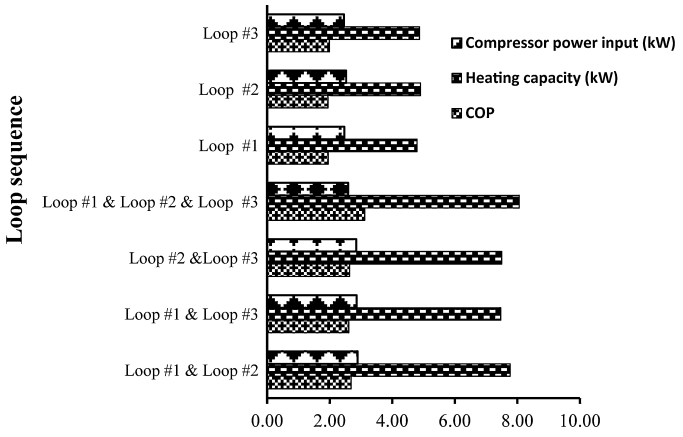

Fig. 16. Average Q_h, W_c and COP of the DX heat pump versus with loop-activated (Test No. 11).

According to Fig. 16, the averages of the heating capacity, power consumed by the compressor and coefficient of performance are respectively around 7.58 kW, 2.87 kW and 2.65 for the two-active-loop sequences, around 8.07 kW, 2.59 kW and 3.12 for three-active-loop sequences, and 4.86 kW, 2.48 kW and 1.96 for the sequences with only one active loop. As can be seen in Fig. 16, the best system performance is achieved when two or three loops are active.

Finally, for the database resulting from eleven tests and that is used to build the ANN model for DX heat pump, Table 4 shows the range of inputs and outputs.

These data can help in adapting the activation of control of loops, depending on the heating load, and finally they allow the optimization of the DX heat pump used for best efficiency.

Table 4
Range of inputs/outputs.

	Minimum	Maximum
T_{wi}	16.6	53.3
P_{fi}	457	1926
T_{fi}	−1.5	19.2
P_{fo}	208	487
T_{fo}	−20.1	8.7
P_{dis}	1141	2459
W_c	1.72	3.17
Q_h	3.7	12.3

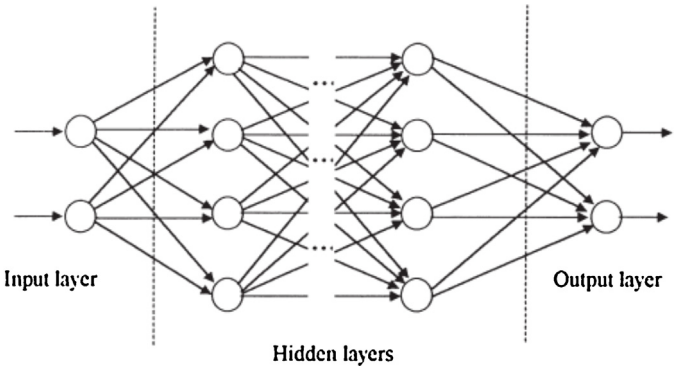

Fig. 17. Schematic diagram of a multi-layer feed forward neural network.

4. Modeling of DX heat pump using ANN

The database obtained from the experimental strategy described in Section 3.1 was used to establish the ANN model of the DX heat pump. Outputs are the coefficient of performance and heating capacity in heating mode. This prediction is important in the optimization, design, integration and control of the thermal system for a long-term use process.

Although the literature contains several network architectures of artificial neurons, the most used network, which is adopted in this study, is the multi-layer feed-forward network shown schematically in Fig. 17. No standard rule exists for choosing the number of hidden layers, or the number of neurons it contains. Usually, the latter are obtained by training. In this study, a single hidden layer was adopted. The back-propagation learning algorithm was used with its variants: the Levenberg–Marquardt (LM), scaled conjugate gradient (SCG), Pola–Ribiere conjugate gradient (CGP) and quasi-Newton back propagation (BFG) algorithms were each tested with a variable neuron number in a hidden layer to choose the most suitable. Because data entries contain negative values, the tangent sigmoid transfer function whose expression is shown below (Eq. (3)) was chosen.

$$f(z) = \frac{1 - e^{-2z}}{1 + e^{-2z}} \tag{3}$$

z is the weighted sum of the input.

The input and output were normalized in the [−1, 1] range. 70% (13,996 data) of data were used for the training and 30% (5999 data) were used to test the model according to the recommendations of Mohanraj et al. [4]. The input variables and output are arranged in an overall architecture shown in Fig. 18. The simulation and processing methodology used throughout this modeling are shown in Fig. 19.

Two programs (one for training and one for testing) were run in the Matlab software environment in conducting this study. The training program includes a random data mix module to prevent the network from learning how the database was established.

To choose the best architecture that fits into our study, statistical performance calculations were carried out. Three statistical parameters were used to assess the performance of each algorithm: the root-mean square (RMS), the coefficient of multiple determinations (R^2) and the coefficient of variation (COV), presented by Eqs. (4)–(6) [4].

$$\mathrm{RMS} = \left(\frac{\sum_{i=1}^{n} (y_i - x_i)^2}{n} \right)^{1/2} \tag{4}$$

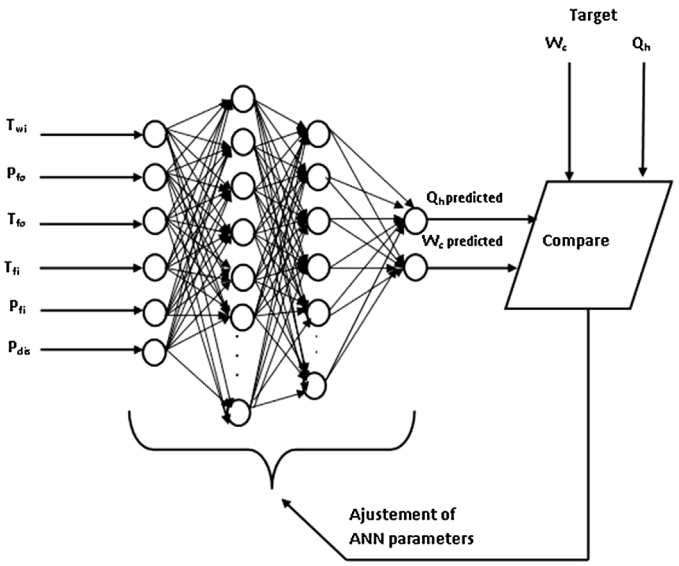

Fig. 18. Training ANN architecture for DX heat pump.

$$R^2 = 1 - \frac{\sum_{i=1}^{n}(y_i - x_i)^2}{\sum_{i=1}^{n} x_i^2} \quad (5)$$

$$\mathrm{COV} = 100\frac{\mathrm{RMS}}{|\bar{x}|} \quad (6)$$

n is the number of test patterns in the test data set; y_i is the value predicted by the ANN model; x_i is the measured value of one data point i; $\bar{x}$ is the mean for all measured data points.

The best architecture is one that offers minimum RMS and COV but the highest value of R^2.

5. ANN results and discussion

The inputs and outputs of the DX heat pump model are presented in preceding chapter. Given the large number of data sets to be processed, we set out to model the DX heat pump with a number of neurons in the hidden layer less than 30, while respecting the model performance criteria; i.e., to obtain a greater coefficient of correlation and have the RMS and COV be as small as possible. Thus, to select the number of neurons in the hidden layer and the best algorithm during the learning phase, simulations were conducted for a number of neurons between 6 and 30. Six is the number of inputs, and represent the minimum value in the hidden layer used in this study.

Table 5 shows the variations in performance parameters of the model during the training phase using the LM algorithms. In accordance with the performance criteria, we can deduce for the two outputs studied, the highest value of R^2, and the smallest values of RMS and COV are obtained for the number of neurons in the hidden layer equal to 28. In this case, the coefficient of determination reaches 0.9995 for W_c and 0.9993 for Q_h with RMS of about 0.0620 and COV of about 2.2513 for W_c and RMS of about 0.2157 and COV of about 2.8648 for Q_h.

By proceeding in a similar fashion for the other three algorithms, Table 6 summarizes the best values of the number of neurons in the hidden layer, the parameter values of performance and the calculation time associated with each of the algorithms.

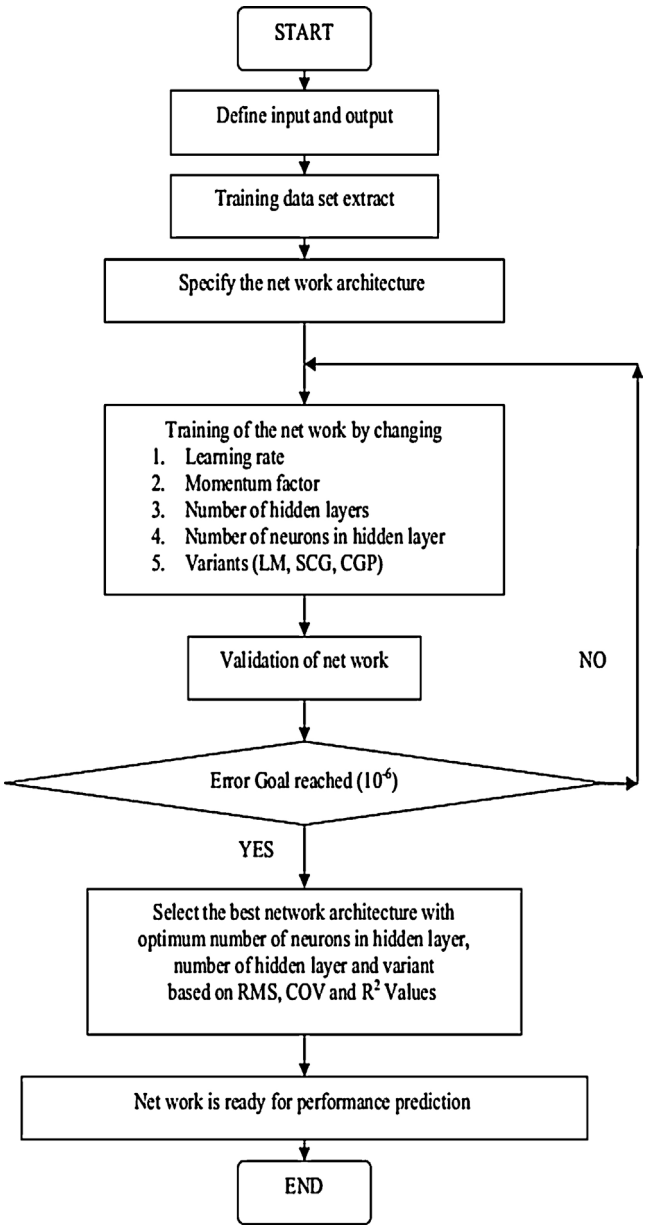

Fig. 19. Flow chart of ANN training process.

Table 5
Training performance versus number in hidden layer for LM.

N	LM					
	W_c			Q_h		
	R^2	RMS	COV	R^2	RMS	COV
6	0.9992	0.0784	2.8468	0.9988	0.2878	3.8219
8	0.9991	0.0853	3.0966	0.9989	0.2737	3.6355
10	0.9992	0.0766	2.7797	0.9991	0.2503	3.3239
12	0.9989	0.0932	3.3824	0.9986	0.3034	4.0288
14	0.9994	0.0662	2.4044	0.9991	0.2399	3.1861
16	0.9994	0.0700	2.5428	0.9991	0.2499	3.3184
18	0.9994	0.0655	2.3794	0.9992	0.2341	3.1090
20	0.9994	0.0659	2.3928	0.9992	0.2306	3.0627
22	0.9994	0.0664	2.4119	0.9992	0.2345	3.1145
24	0.9994	0.0671	2.4365	0.9991	0.2393	3.1777
26	0.9993	0.0732	2.6572	0.9991	0.2460	3.2673
28	0.9995	0.0620	2.2513	0.9993	0.2157	2.8648
30	0.9991	0.0826	2.9969	0.9983	0.3342	4.4388

Table 6
Best number in hidden layer and calculi time versus algorithm in training.

		LM	CGP	SCG	BFG
	BNHL	28	30	24	28
	T_s	78	79	109	91
W_c	R^2	0.9995	0.9984	0.9986	0.9992
	RMS	0.0620	0.1105	0.1010	0.0778
	COV	2.2513	4.0123	3.6685	2.8214
Q_h	R^2	0.9993	0.9981	0.9982	0.9987
	RMS	0.2157	0.3582	0.3450	0.2886
	COV	2.8648	4.7593	4.5783	3.8278

Table 7
Performance of the two best algorithms during validation.

		LM28	BFG28
W_c	R^2	0.9994	0.9991
	RMS	0.0676	0.0864
	COV	2.4520	2.9257
Q_h	R^2	0.9989	0.9986
	RMS	0.2590	0.3009
	COV	3.4118	3.9795

According to Table 6, LM appears to be the best training algorithm because the performance coefficients (R^2, RMS COV) obtained are the best compared to other algorithms used in this study, followed by the BFG algorithm, SCG, and finally, the CGP algorithm. LM with 28 neurons in its hidden layer offers the smallest time calculation versus the other three algorithm calculations, thus making it the fastest. The CGP algorithm also appears to be quite fast, but the RMS and COV are higher.

All in all, it is concluded that among the four algorithms tested in this study, LM with 28 (LM28) neurons in the hidden layer, is the first algorithm that models the data of the DX heat pump. The second best algorithm is the BFG with the same number of neurons in the hidden layer (BFG28).

Table 7 shows the results of validation tests for remaining data (5999, 30%) for the two best algorithms identified in this study. The test shows that LM28 is still the best algorithm, and it will be retained for the modeling of the DX heat pump and for our future works on the DX heat pump presented in this study. The relatively low values of COV (2.45 for the W_c and 3.41 for Q_h) and RMS (0.07 for W_c and 0.26 for Q_h) therefore reflect small residuals compared to the values predicted by the model and suggests a good model fit.

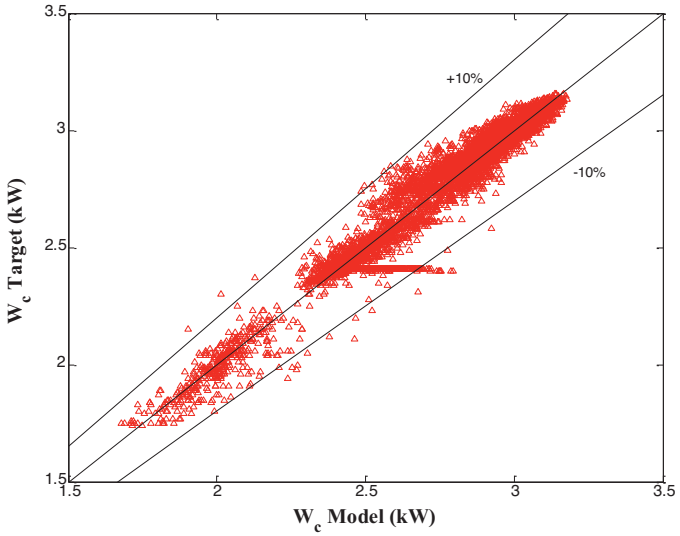

Fig. 20. Model validation with LM28 for W_c.

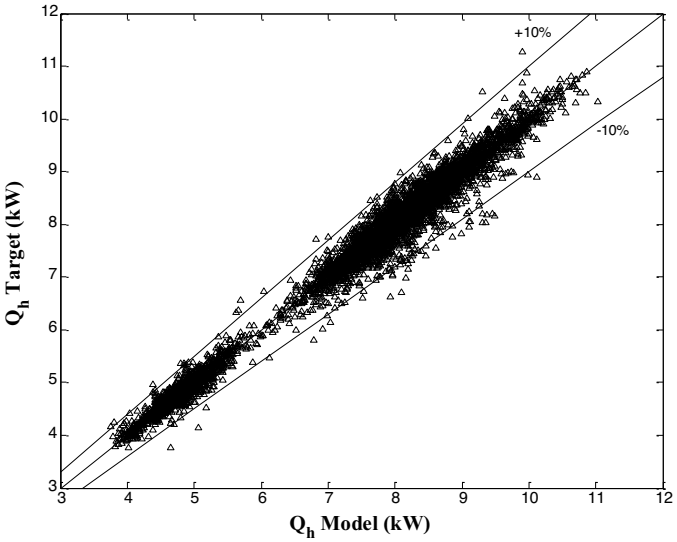

Fig. 21. Model validation with LM28 for Q_h.

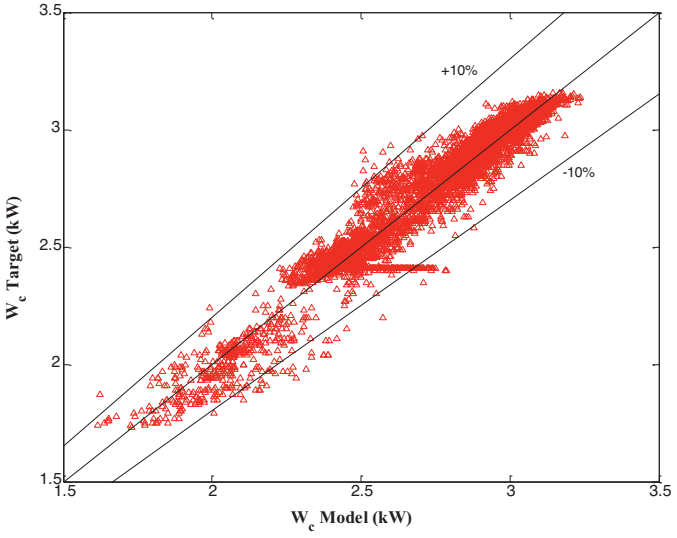

Fig. 22. Model validation with BFG28 for W_c.

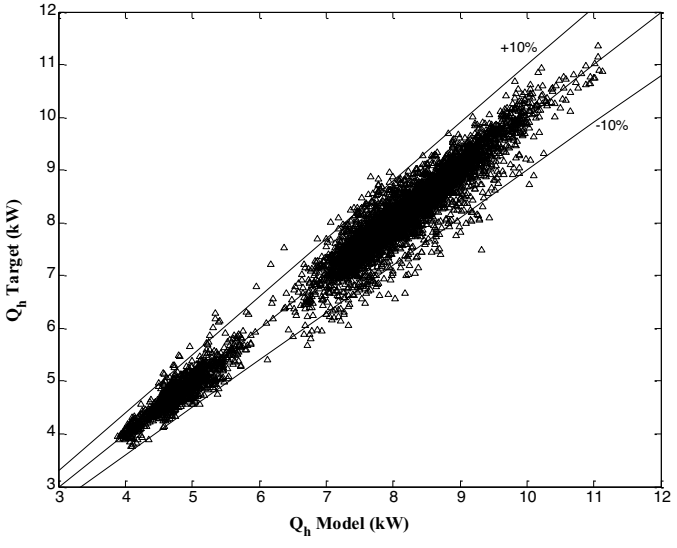

Fig. 23. Model validation with BFG28 for Q_h.

This is confirmed by the relatively high values of the coefficients of multiple determinations obtained (0.9994 for W_c and 0.9989 for Q_h).

Figs. 20–23 shows the results of validation carried out with LM28 and BFG28.

As can be seen from these figures, the predicted values appear approximated well the experimental values. LM28 provided the best results.

6. Conclusion

The objective of this study was to predict the performances (compressor power consumption and heating capacity) of a DX geothermal heat pump using artificial neural networks. At the end of this investigation, it can be summarized that:

- The work has highlighted an experimental strategy for data collection which has served to establish an ANN model of the DX heat pump. The data obtained can also be used to control and adapt the activation geothermal loops, depending on heat demand, for a more efficient use.
- The input of the ANN model takes into account the thermodynamic parameters that influence the performance of the DX heat pump: cooling water inlet temperature, the temperature and pressure at the inlet/outlet of the geothermal evaporator and the discharge pressure.
- Among the four cases of the algorithms tested in the modeling process, the LM with 28 neurons appears to be the best and fastest despite the large number of data to be processed. This prediction model obtained is very satisfactory (the coefficients of multiple determinations has an average of about 0.9991, with an average RMS of 0.16330, and an average COV of 2.9319) for the two outputs, and therefore proves that ANN is a good alternative approach in modeling complex systems.

This interesting study on both the experimental and modeling is one of the references in the field of DX heat pumps and will help readers build their own work.

Future work will focus on the implementation of the best strategies to control the DX heat pump operations using the behavioral model presented in this study and thus contribute to its valuation.

Acknowledgements

Financial support for this study was provided by the Canadian Department of Natural Resources (CanmetEnergy), École de technologie supérieure and its financial partners. The authors would like to gratefully acknowledge their invaluable contributions. In addition, the valuable comments of the reviewers are gratefully acknowledged.

References

[1] M.W. Gardner, S.R. Dorling, Artificial neural networks (the multilayer perceptron) – a review of applications in the atmospheric sciences, Atmospheric Environment 32 (14–15) (1998) 2627–2636.
[2] S.A. Kalogirou, Applications of artificial neural networks in energy systems, Energy Conversion and Management 40 (10) (1999) 1073–1087.
[3] I.A. Basheer, M. Hajmeer, Artificial neural networks: fundamentals, computing, design, and application, Journal of Microbiological Methods 43 (1) (2000) 3–31.
[4] M. Mohanraj, S. Jayaraj, C. Muraleedharan, Applications of artificial neural networks for refrigeration, air-conditioning and heat pump systems – a review, Renewable and Sustainable Energy Reviews 16 (2) (2012) 1340–1358.
[5] H. Esen, M. Inalli, Modelling of a vertical ground coupled heat pump system by using artificial neural networks, Expert Systems with Applications 36 (7) (2009) 10229–10238.
[6] R. Kumar, R.K. Aggarwal, J.D. Sharma, Energy analysis of a building using artificial neural network: a review, Energy and Buildings 65 (2013) 352–358.
[7] E. Arcaklıoğlu, A. Çavuşoğlu, A. Erişen, Thermodynamic analyses of refrigerant mixtures using artificial neural networks, Applied Energy 78 (2) (2004) 219–230.
[8] Y. Guo, G. Zhang, J. Zhou, J. Wu, W. Shen, A techno-economic comparison of a direct expansion ground-source and a secondary loop ground-coupled heat pump system for cooling in a residential building, Applied Thermal Engineering 35 (2012) 29–39.
[9] S. Kavanaugh, K. Rafferty, Ground-source Heat Pumps: Design of Geothermal Systems for Commercial and Institutional Buildings, 1997.
[10] A. Capozza, M. De Carli, A. Zarrella, Design of borehole heat exchangers for ground-source heat pumps: a literature review, methodology comparison and analysis on the penalty temperature, Energy and Buildings 55 (2012) 369–379.
[11] K. Nagano, T. Katsura, S. Takeda, Development of a design and performance prediction tool for the ground source heat pump system, Applied Thermal Engineering 26 (14–15) (2006) 1578–1592.
[12] F. Robert, L. Gosselin, New methodology to design ground coupled heat pump systems based on total cost minimization, Applied Thermal Engineering 62 (2) (2014) 481–491.
[13] W. Gang, J. Wang, Predictive ANN models of ground heat exchanger for the control of hybrid ground source heat pump systems, Applied Energy 112 (2013) 1146–1153.
[14] J. Teeter, C. Mo-Yuen, Application of functional link neural network to HVAC thermal dynamic system identification, IEEE Transactions on Industrial Electronics 45 (1) (1998) 170–176.
[15] J.-L. Fannou, C. Rousseau, L. Lamarche, K. Stanislaw, Experimental analysis of a direct expansion geothermal heat pump in heating mode, Energy and Buildings 75 (2014) 290–300.
[16] H. Esen, M. Inalli, ANN and ANFIS models for performance evaluation of a vertical ground source heat pump system, Expert Systems with Applications 37 (12) (2010) 8134–8147.
[17] K.J. Hunt, D. Sbarbaro, R. Żbikowski, P.J. Gawthrop, Neural networks for control systems – a survey, Automatica 28 (6) (1992) 1083–1112.
[18] R. Pierre, S. Fabrice, B. Lionel, Régulation d'un processus industriel par réseaux de neurones Techniques de l'ingénieur Automatique avancée, base documentaire: TIB393DUO (ref. article: s7582), 2001.
[19] H. Guang-Bin, Z. Qin-Yu, S. Chee-Kheong, Real-time learning capability of neural networks, neural networks, IEEE Transactions on Industrial Electronics 17 (4) (2006) 863–878.
[20] J.-L. Fannou, C. Rousseau, L. Lamarche, K. Stanislaw, Optimisation d'une pompe à chaleur géothermique à expansion directe(DX) par la méthode Taguchi, Récents Progrès en Génie des Procédés 104 (2013).
[21] S. Gunes, E. Manay, E. Senyigit, V. Ozceyhan, A Taguchi approach for optimization of design parameters in a tube with coiled wire inserts, Applied Thermal Engineering 31 (14–15) (2011) 2568–2577.